

Shape optimization of acoustic horns using the multimodal method

Hao Dong, Yong Shen,^{a)} and Hao Gao

Key Laboratory of Modern Acoustics (MOE), Institute of Acoustics, Nanjing University,
Nanjing, 210093, China
hdongnju@gmail.com, yshen@nju.edu.cn, hgao@smail.nju.edu.cn

Abstract: This paper presents a method for the shape optimization of an acoustic horn with respect to the impedance matching property based on the discrete multimodal method. The method models the horn as a series of short cylinders and takes mode coupling across the discontinuities into account. The optimization employs a gradient-based algorithm, and allows for analytical derivation of the objective function and its gradient in a numerically workable manner. A case study followed with an experimental validation is presented. With appropriate parameter settings, the method is capable of rapidly finding a smooth and convex horn design that behaves like a high-pass radiator with near-ideal wideband transmission in small dimensions. © 2020 Acoustical Society of America

[Editor: Charles C. Church]

Pages: EL326–EL332

Received: 21 December 2019 Accepted: 16 March 2020 Published Online: 9 April 2020

1. Introduction

Loudspeaker horns can provide impedance matching and radiate sound efficiently; hence, they are widely used as components in loudspeaker systems.^{1,2} Previous studies^{3,4} have shown that the impedance matching property of the horn is very sensitive to its shape and numerical optimization can be used to design very efficient horns within a desired frequency range. In the existing works,^{3–7} wave propagation is modeled by the finite element method (FEM) or boundary element method, and the minimization problem is solved using gradient-based or zeroth-order algorithms. However, the element-based models require detailed discretization of the domain or the horn walls and are therefore usually time consuming.

This paper presents a horn optimization method that combines the discrete multimodal decomposition method^{8,9} with a gradient-based algorithm. The discrete multimodal method has been used in the study of wave propagation in brass musical instruments¹⁰ and in the horn loudspeaker simulation, which proves to be an accurate and efficient semi-analytical method.¹¹ The sampled horn radii depicting the profile of the axisymmetric horn are directly used as design variables. Therefore, the optimization allows for a large number of variables. Moreover, accuracy can be easily adjusted by changing the number of segments and modes. The objective function and its derivatives can be determined analytically, enabling rapid computation of the gradient. The optimization problem is formulated as an unconstrained nonlinear least squares problem and solved by the Levenberg–Marquardt algorithm. To overcome numerical difficulties in projecting the impedance matrix across a contracting discontinuity, we propose an improved equation that is numerically workable. Another objective of the research is to provide a design example and the resulting optimized shape that is of practical use for near-ideal wide-band energy transmission.

The rest of the paper is organized as follows: Sec. 2 presents the derivation of the objective function and its gradient based on the discrete multimodal method, and the formulation of the optimization problem. In Sec. 3 a case study is presented, where a wideband highly efficient horn is designed and studied experimentally. Section 4 contains the concluding remarks and scope for further research.

2. Method

2.1 Discrete multimodal decomposition method

Consider an axisymmetric horn of length L terminated in an infinite baffle, with a rigid wall of arbitrary shape. The horn can be approximated by a series of short cylinders, as shown in Fig. 1(a). By assuming steady-state axisymmetric wave propagation and omitting a time

^{a)} Author to whom correspondence should be addressed.

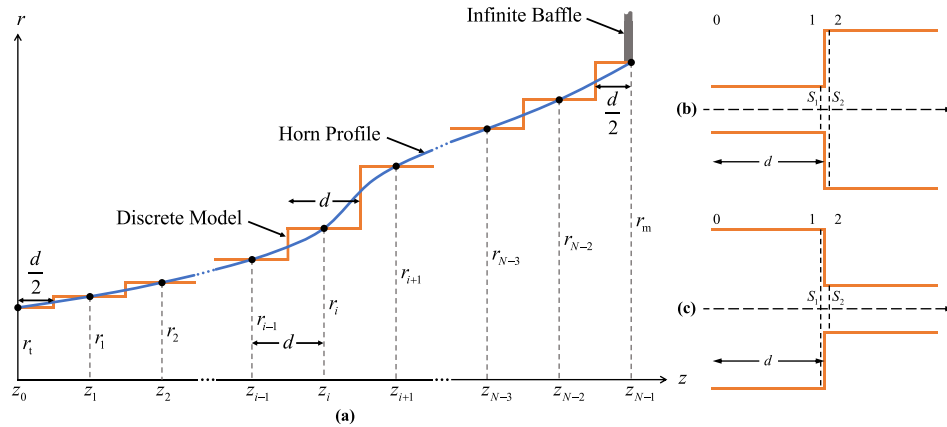


Fig. 1. (Color online) (a) An axisymmetric horn of arbitrary profile approximated by a series of short cylinders. Along the z axis (direction of wave propagation), the horn radius function $r(z)$ is sampled at N equally spaced points z_0 to z_{N-1} [the sampling interval is $d = L/(N-1)$], and N coaxial cylindrical sections are created. The throat of the horn is located at z_0 of radius r_t , and the mouth at z_{N-1} of radius r_m . (b) Expanding discontinuity geometry. (c) Contracting discontinuity geometry.

harmonic factor of $e^{i\omega t}$, the pressure p and axial velocity v_z in any short cylinder can be expressed as a weighted sum of the transverse modes of the cylindrical waveguide. That is, $p = \mathbf{P}^T \mathbf{\Psi}$, $v_z = (1/S) \mathbf{U}^T \mathbf{\Psi}$, where $\mathbf{\Psi}$ is a vector consisting of eigenfunctions, \mathbf{P} and \mathbf{U} are vectors consisting of the modal amplitudes projected over the eigenfunctions, and $S = \pi R^2$ is the cross-sectional area. The eigenfunction is $\psi_n(r) = [J_0(\gamma_n r/R)/J_0(\gamma_n)]$, where γ_n are the successive zeros of the Bessel function of order one. The multimodal impedance matrix is defined as \mathbf{Z} , such that $\mathbf{P} = \mathbf{Z}\mathbf{U}$. The projection of the impedance matrix across a discontinuity and across a cylinder under the following two cases is presented.

(i) The cross-section of the adjacent cylinders expands across the discontinuity,¹⁰ i.e., $S_1 < S_2$, as shown in Fig. 1(b). The impedance matrix on surface 1 can be found from the impedance matrix on surface 2

$$\mathbf{Z}^{(1)} = \mathbf{F}\mathbf{Z}^{(2)}\mathbf{F}^T, \quad (1)$$

where the matrix \mathbf{F} is defined by $F_{nm} = [2\beta\gamma_m J_1(\beta\gamma_m)/(\beta^2\gamma_m^2 - \gamma_n^2)J_0(\gamma_n)]$, $\beta = R_1/R_2$ is the radius ratio, and $F_{11} = 1$. Next, we determine the impedance matrix on surface 0 from the following equation proposed by Roure,⁸ which is numerically workable:

$$\mathbf{Z}^{(0)} = \mathbf{D}_3^{-1}\mathbf{Z}_c - \mathbf{D}_2^{-1}\mathbf{Z}_c(\mathbf{Z}^{(1)} + \mathbf{D}_3^{-1}\mathbf{Z}_c)^{-1}\mathbf{D}_2^{-1}\mathbf{Z}_c, \quad (2)$$

where \mathbf{D}_2 and \mathbf{D}_3 are diagonal matrices with the n th diagonal element given by $i \tan k_n d$ and $i \sin k_n d$, respectively, and $i = \sqrt{-1}$. \mathbf{Z}_c is the characteristic impedance matrix of the cylindrical waveguide with its n th diagonal element given by $k\rho c/k_n S_1$, where k_n is the propagation constant of the n th mode

$$k_n = \begin{cases} \sqrt{k^2 - (\gamma_n/R_1)^2}, & k \geq \gamma_n/R_1; \\ -i\sqrt{(\gamma_n/R_1)^2 - k^2}, & k < \gamma_n/R_1. \end{cases} \quad (3)$$

(ii) The cross-section of the adjacent cylinders contracts across the discontinuity, i.e., $S_1 > S_2$, as shown in Fig. 1(c). In this case, we have

$$\mathbf{Z}^{(1)} = \mathbf{V}^{-1}\mathbf{Z}^{(2)}(\mathbf{V}^T)^{-1}, \quad (4)$$

where the matrix \mathbf{V} is defined by $V_{nm}(\beta) = F_{nm}(1/\beta)$. The \mathbf{V} matrix is close to singular when the radius ratio is large or the number of modes is high.¹¹ Because we desire an unconstrained optimization and do not want to impose any limitation on the change in cross-section, Eq. (4) cannot be used directly. If we use the admittance matrix $\mathbf{Y} = \mathbf{Z}^{-1}$, the admittance on surface 1 can be found without inverting the \mathbf{V} matrix,

$$\mathbf{Y}^{(1)} = \mathbf{V}^T \mathbf{Y}^{(2)} \mathbf{V}. \quad (5)$$

However, when using Eq. (2) to find the impedance matrix on surface 0, there may still be numerical problems involved in inverting $\mathbf{Y}^{(1)}$. To overcome this problem, we derive a numerically workable matrix projection equation that directly uses $\mathbf{Y}^{(1)}$,

$$\mathbf{Z}^{(0)} = \mathbf{D}_3^{-1} \mathbf{Z}_c - \mathbf{D}_1^{-1} (\mathbf{Y}^{(1)} + \mathbf{D}_3 \mathbf{Y}_c)^{-1} \mathbf{D}_1^{-1}, \quad (6)$$

where \mathbf{D}_1 is a diagonal matrix with its n th diagonal element given by $\cos k_n d$, and $\mathbf{Y}_c = \mathbf{Z}_c^{-1}$ is the characteristic admittance matrix of the cylindrical waveguide.

Zorumski¹² analytically derived the impedance matrix \mathbf{Z}_R for radiation from an opening in an infinite baffle. Then, starting from the mouth and by repeatedly using Eqs. (1) and (2) for expanding discontinuity, and Eqs. (5) and (6) for contracting discontinuity (note that the impedance matrix on surface 0 is always invertible), we can find the throat impedance matrix \mathbf{Z}_0 .

2.2 Impedance matching property

The impedance matching property is measured by the throat reflection coefficients. We assume that the throat of the horn is connected to a semi-infinite cylindrical waveguide, and the source is far from the throat with a frequency at which all higher-order modes are evanescent. By decomposing the pressure and velocity modal amplitudes at the throat as the sum of incident and reflected parts, we have $\mathbf{P}_t = \mathbf{P}_+ + \mathbf{P}_-$ and $\mathbf{U}_t = \mathbf{U}_+ + \mathbf{U}_-$, where $\mathbf{U}_+ = (1, 0, 0, \dots)^T$ is the incident part. For horns with low flare rate near the throat, we neglect the higher-order components in the reflected wave. Therefore, the plane-wave pressure reflection coefficient at the throat is $r_p = (Z_t - R_0)/(Z_t + R_0)$, where Z_t is the corner value of the throat impedance matrix \mathbf{Z}_0 , and $R_0 = \rho_0 c / S_t$ is the local characteristic impedance.

However, to rigorously take into account the effects of the higher-order modes, we should calculate the reflection and transmission of the energy flux⁹ of a horn that has been optimized with respect to r_p . First, the reflected part of the volume velocity vector is found by $\mathbf{U}_- = (\mathbf{Z}_c + \mathbf{Z}_0)^{-1} (\mathbf{Z}_c - \mathbf{Z}_0) \mathbf{U}_+$. Then, the energy flux reflection coefficient is $r_W = \text{Re}(\mathbf{U}_-^T \mathbf{Z}_c \mathbf{U}_-^*) / R_0$. The transmission coefficient or transmission efficiency is $t_W = 1 - r_W$. The energy flux reflection coefficient can also be used as the objective function.

2.3 Objective function and gradients

In this work, the length of the horn and the radii of the throat and mouth are fixed, and the optimization only focuses on the horn-flare shape. The objective function is defined as the square sum of the magnitude of the pressure reflection coefficient at multiple specified frequencies in a target frequency range

$$J(\mathbf{r}) = \sum_{i=1}^M |r_p(\mathbf{r}; f_i)|^2, \quad (7)$$

where $\mathbf{r} = (r_1, r_2, \dots, r_{N-2})^T$ is the design variable consisting of the sampled radii, and f_1, f_2, \dots, f_M are M considered frequencies. Although the finite difference approximation can be used to evaluate the gradients, the round-off and truncation error can significantly decrease the accuracy and efficiency of the optimization. The multimodal method allows the analytical derivation of the gradients. The derivative of the pressure reflection coefficient with respect to the variable is expressed as $(\partial r_p / \partial \mathbf{r}) = [2R_0 / (Z_t + R_0)^2] (\partial Z_t / \partial \mathbf{r})$, where Z_t and $\partial Z_t / \partial \mathbf{r}$ are found by the throat impedance matrix and its derivatives, respectively. To achieve this, the impedance matrix at the left hand of each segment is denoted as \mathbf{Z}_i ($i = 0, 1, 2, \dots, N-1$). We first calculate and store \mathbf{Z}_i and $\partial \mathbf{Z}_i / \partial \mathbf{r}_i$ from the mouth to the throat by directly using and differentiating Eqs. (1), (2), (5), and (6), and then calculate $\partial \mathbf{Z}_0 / \partial \mathbf{r}_i$.

2.4 Optimization problem

To avoid irregular shapes, we apply two smoothing strategies.^{3,4} The first is Tikhonov regularization, which is a common way to remedy the problem with non-smooth solutions. A regularization term $\varepsilon \int_{z_0}^{z_{N-1}} \eta(z)^2 dz$ is added to the objective function, where $\eta(z) = r''(z)$ is the curvature of the shape, and ε is an adjustable regularization parameter. A discrete version of this term is $(\varepsilon MN^3 / L^3) \mathbf{x}^T \mathbf{x}$, where \mathbf{x} is the second-order difference of the radius vector \mathbf{r} . The variable substitution relationship is given by

$$\mathbf{x} = \mathbf{K} \mathbf{r} + \mathbf{b}, \quad (8)$$

where

$$K = \begin{pmatrix} -2 & 1 & 0 & \cdots & 0 \\ 1 & -2 & \ddots & \ddots & \vdots \\ 0 & \ddots & \ddots & \ddots & 0 \\ \vdots & \ddots & \ddots & -2 & 1 \\ 0 & \cdots & 0 & 1 & -2 \end{pmatrix}$$

is a tridiagonal matrix of order $N - 2$ and $\mathbf{b} = (r_t, 0, 0, \dots, 0, r_m)^T$. The second strategy is to use \mathbf{x} directly as the design variable. Then, the optimization problem is formulated as

$$\min_{\mathbf{x}} \left[\sum_{i=1}^M |r_p(\mathbf{x}; f_i)|^2 + \frac{\varepsilon MN^3}{L^3} \mathbf{x}^T \mathbf{x} \right]. \quad (9)$$

The derivatives with respect to \mathbf{x} can be found from the chain rule $(\partial/\partial \mathbf{x}) = (\partial/\partial \mathbf{r}) \mathbf{K}^{-1}$ (in numerator layout).

To maximize the search space, no constraints are imposed on the design variable. The Levenberg–Marquardt algorithm, implemented by the MATLAB `lsqnonlin` solver, is used to solve the optimization problem. Iterations end when the relative change in the value of the objective function or the norm of the variable is smaller than 1×10^{-6} in a step.

3. Design and measurement of a wideband highly efficient horn

3.1 Parameter settings and optimization results

A design example is presented in this section. Our task is to design a wideband efficient horn that is also capable of good low-frequency radiation in small dimensions. The cutoff frequency above which a horn is an efficient radiator is limited by its dimensions. The plane-wave theory of the horn shows that the exponential horn (the cross-sectional area varies as $S(z) = S_0 e^{mz}$, m is the flare constant) has good low-frequency behavior,¹ and the optimal impedance matching of a finite-length exponential horn radiating into half space is achieved when $k_c r_m = 1$, where $k_c = (m/2) = (2\pi f_c/c)$, f_c is the cutoff frequency, and c is the speed of sound.¹³ Therefore, we set the fixed parameters r_t , r_m , and L according to an “optimal” exponential horn as summarized in Table 1, rather than setting them arbitrarily. The throat radius is intended for a 1-in. compression driver. The mouth radius and the length are set to satisfy $k_c r_m = 1$ as the horn flares exponentially. The exponential horn, which is used as the initial shape for optimization, has a cutoff frequency of 680 Hz. The optimization is carried out at 37 logarithmically spaced frequencies in the range of 2–16 kHz (frequency interval of 1/12th octave), which is within the passband of the exponential horn, as listed in Table 1. First, a preliminary optimization is performed using 5 modes and 128 horn segments. Then, we use the intermediate shape to perform a precise optimization with 21 modes and 256 segments to obtain the final optimized shape. A regularization parameter of $\varepsilon = 2.5 \times 10^{-10}$ is applied during the two-step optimization. Total computational time is about 1.2 h on a personal computer.

Figure 2(a) shows the initial and optimized horn shapes. The optimized shape is smooth and convex, with a flare rate that gradually increases along the axis. The reflection coefficient and transmission efficiency of the two horns are computed with 128 modes and 1024 segments with a frequency resolution of 1/18th octave, as shown in Figs. 2(b) and 2(c), respectively. We can see that the pressure reflection coefficient of the optimized horn is much lower than the exponential horn in the target frequency range. The optimized horn exhibits almost perfect transmission efficiency above 2 kHz with a smooth transition band. In contrast, the transmission efficiency of the exponential horn has larger ripples and greater efficiency losses. However, the –3 dB lower cutoff frequency in the transmission efficiency of the optimized horn (about 1000 Hz) is higher than that of the exponential horn (about 700 Hz).

A drawback to Tikhonov regularization is the difficulty in selecting a suitable value of ε , which should guarantee both the transmission efficiency and shape smoothness. Fortunately, a reasonable range for this value can be quickly determined in the preliminary step since this step can be done in a few minutes. The number of modes and segments used in the precise step determine the accuracy of the final design. In this example, the reflection coefficient of the optimized

Table 1. The dimensions of the horn and the frequencies used in the optimization.

r_t (m)	r_m (m)	L (m)	f (Hz)
0.0127	0.0810	0.15	$2000 \times 2^{i/12}$, $i = 0, 1, \dots, 36$

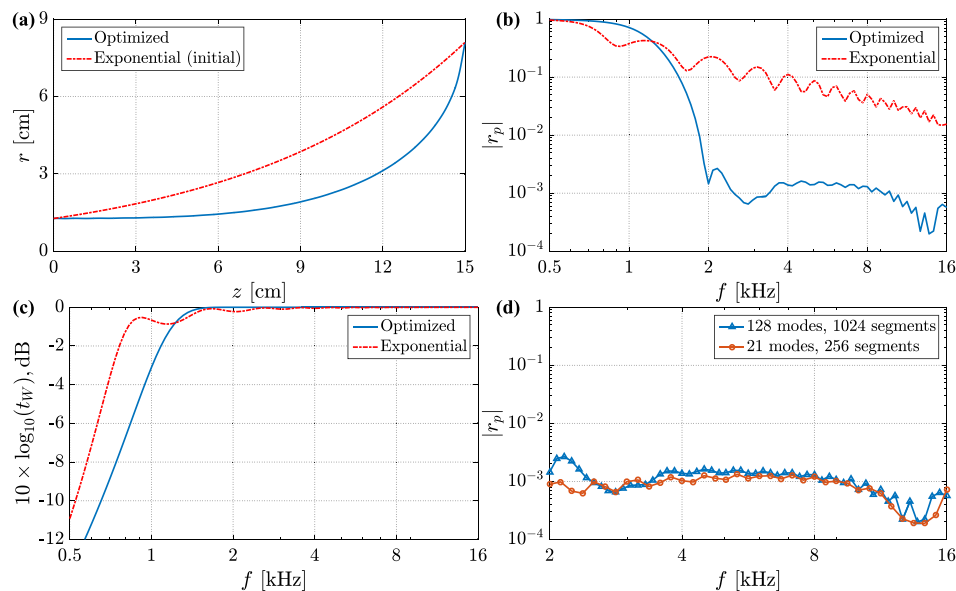


Fig. 2. (Color online) (a) Shapes of the initial and optimized horns. (b) Comparison of pressure reflection coefficients. (c) Comparison of transmission efficiencies. (d) Comparison of reflection coefficients of the optimized horn obtained directly from the optimization process with those calculated with higher accuracy [the same as in (b)] in the design band.

horn obtained directly from the optimization process acceptably agree with that calculated with a higher accuracy, as shown in Fig. 2(d). If not, more precise optimizations can be done by including more modes and variables in the second step, until the result meets the specific requirement of the design task, at the cost of an increased computational load.

3.2 Measurement

The pressure reflection coefficient of the optimized horn was measured using the setup shown in Fig. 3(a). The mouth of the horn was mounted on a standard baffle in an anechoic chamber. The throat of the horn was connected to a 300-mm-long 12.7-mm-radius cylindrical waveguide, of which the other end was excited by a 1-in. compression driver (SMC225/ND, Beyma, Spain). A step sine signal generated by the PULSE Analyzer (Type 3160 A, Brüel & Kjær, Denmark),

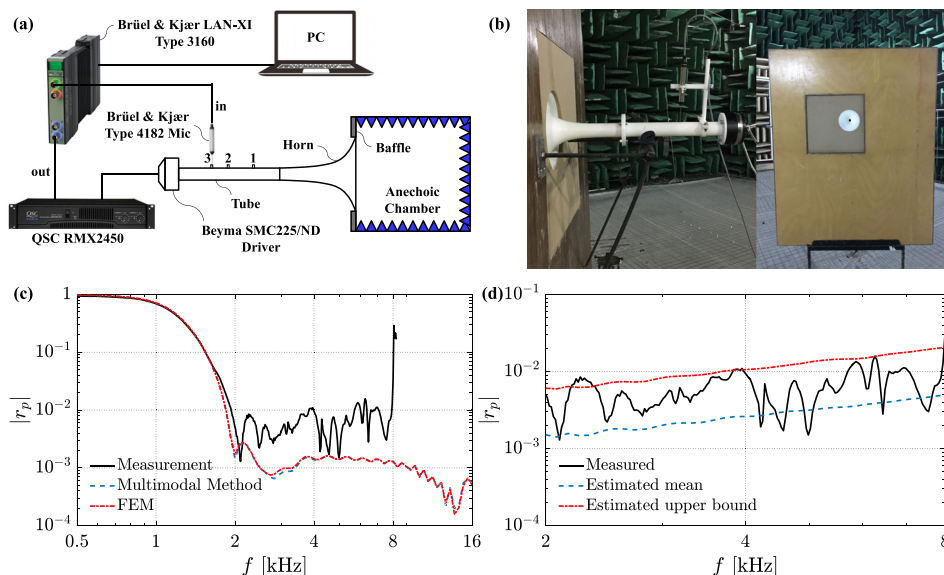


Fig. 3. (Color online) (a) Schematic of measurement setup; (b) images of setup; (c) comparison of measured and theoretical pressure reflection coefficient; the theoretical curve is also confirmed with FEM. (d) The effect of manufacturing deficiencies on the reflection coefficient. Each radius is a random variable following a normal distribution with a mean of the optimized radius and a standard deviation of one-sixth of the manufacturing tolerance. Tolerance of the reflection coefficient is set to be six standard deviations. The lower bound of tolerance interval is less than zero and not shown, only the mean and upper bound are shown.

ranging from 500 Hz to 8 kHz, was sent to the driver after amplification by a power amplifier (RMX2450, QSC, Costa Mesa, CA). The cutoff frequency of the cylindrical waveguide is determined by $f_{cw} = (\lambda c / 2\pi r_t) \approx 7.99$ kHz, where $\lambda = 1.841$ is the eigenvalue corresponding to the first non-axisymmetric mode, and $c = 346.2$ m/s. Hence, in the measured frequency range, the wave field near the throat of the horn inside the waveguide can be approximately regarded as planar. As is shown in Fig. 3(b), the pressure at distances of $s_1 = 11$ cm, $s_2 = 16$ cm, and $s_3 = 19$ cm away from the throat of the horn was measured with a probe microphone (type 4182, Brüel & Kjær, Denmark). Then, we have

$$\begin{pmatrix} p_1 \\ p_2 \\ p_3 \end{pmatrix} = \begin{pmatrix} e^{jks_1} & e^{-jks_1} \\ e^{jks_2} & e^{-jks_2} \\ e^{jks_3} & e^{-jks_3} \end{pmatrix} \begin{pmatrix} A \\ B \end{pmatrix}, \quad (10)$$

where p_1 , p_2 , and p_3 are the pressure at three measurement points, respectively. A and B are the complex amplitude of the incident and reflected waves, respectively, and k is the wavenumber. The values of A and B were evaluated by Eq. (10) with the least squares method. Thus, the magnitude of the reflection coefficient is $r_p = |B/A|$. The measured and theoretical results are compared in Fig. 3(c). The average value of the measured reflection coefficient from 2 to 8 kHz is 6.1×10^{-3} . The effect of deviation of the shape due to manufacturing deficiencies (manufacturing tolerance is $200 \mu\text{m}$) is evaluated by computing the reflection coefficients of 1000 noise-perturbed horn shapes. Curves of the mean and upper bound of tolerance are shown in Fig. 3(d), indicating that the discrepancies between the measured and theoretical results are partly due to the manufacturing tolerance. Other possible sources of error include the least square fit residual, finite baffle size, and horn modeling assumptions.

Although the range of 8 to 16 kHz still falls into the design band and is below the cut-off frequency of the first axisymmetric higher-order mode of the waveguide (16.62 kHz), application of the measurement method in this range yielded a sudden increased reflection coefficient in a level much higher than in 2–8 kHz, which implies the propagation of the non-axisymmetric modes in the waveguide and the measurement method was therefore invalid. This may be caused by the defect of axisymmetry of the waveguide-horn system and excitation of non-axisymmetric modes by the compression driver. To verify the performance of the optimized horn in this frequency range, a FEM simulation was performed using COMSOL Multiphysics. The result is also shown in Fig. 3(c), which agrees well with the multimodal method in the entire frequency range.

4. Conclusion

This paper proposes a method for the optimization of loudspeaker horns with respect to the impedance matching property. Based on the discrete multimodal method, it is convenient to introduce a large number of design variables that directly depict the horn profile. Pressure reflection coefficient and its gradient of an axisymmetric horn of arbitrary shape can be found analytically without numerical problems. Under suitable parameter settings, the algorithm converges fast to a shape with acceptable smoothness and improved transmission efficiency over the desired frequency range. One limitation of the present study is that the length of the horn and the radii of the throat and mouth are fixed. In the optimization example, we pre-specified the fixed parameters based on some earlier observations to seek an optimal result in small dimensions. The comparison between the optimized horn and the exponential horn indicates that for horns with the same dimensions, highly efficient energy transmission combined with a flat response in the pass-band is traded off against its relatively high cutoff frequency. The convenience of the multimodal optimization method makes it possible to further investigate the physical limitations of the low-frequency radiation characteristics, dimensions, and efficiency of the horn. The method is also suitable for horn optimization with respect to far-field directivity patterns, which is also of practical importance in horn loudspeaker applications.

Acknowledgments

This work was supported by the National Key R&D Program of China under Grant No. 2018YFB1403800.

References and links

- ¹L. L. Beranek and T. J. Mellow, *Acoustics: Sound Fields and Transducers* (Academic Press, New York, 2012).
- ²B. Kolbrek and T. Dunker, *High-Quality Horn Loudspeaker Systems: History, Theory and Design* (Kolbrek Elektroakustikk, Rauland, 2019).
- ³E. Bängtsson, D. Noreland, and M. Berggren, "Shape optimization of an acoustic horn," *Comp. Methods Appl. Mech. Eng.* **192**(11–12), 1533–1571 (2003).

- ⁴R. Udawalpola and M. Berggren, "Optimization of an acoustic horn with respect to efficiency and directivity," *Int. J. Numer. Methods Eng.* **73**(11), 1571–1606 (2008).
- ⁵R. Udawalpola, E. Wadbro, and M. Berggren, "Optimization of a variable mouth acoustic horn," *Int. J. Numer. Methods Eng.* **85**(5), 591–606 (2011).
- ⁶R. Barbieri and N. Barbieri, "Acoustic horns optimization using finite elements and genetic algorithm," *Appl. Acoust.* **74**(3), 356–363 (2013).
- ⁷A. Bernland, E. Wadbro, and M. Berggren, "Acoustic shape optimization using cut finite elements," *Int. J. Numer. Methods Eng.* **113**(3), 432–449 (2018).
- ⁸A. Roue, "Propagation guidée: Etude des discontinuités" ("Guided propagation: Study of discontinuities") Ph.D. dissertation, Université Aix-Marseille, 1976.
- ⁹V. Pagneux, N. Amir, and J. Kergomard, "A study of wave propagation in varying cross-section waveguides by modal decomposition. Part I. Theory and validation," *J. Acoust. Soc. Am.* **100**(4), 2034–2048 (1996).
- ¹⁰J. A. Kemp, "Theoretical and experimental study of wave propagation in brass musical instruments," Ph.D. dissertation, The University of Edinburgh, 2002.
- ¹¹B. Kolbrek, "Extensions to the mode matching method for horn loudspeaker simulation," Ph.D. dissertation, Norwegian University of Science and Technology, 2016.
- ¹²W. E. Zorumski, "Generalized radiation impedances and reflection coefficients of circular and annular ducts," *J. Acoust. Soc. Am.* **54**(6), 1667–1673 (1973).
- ¹³D. B. Keele, Jr., "Optimum horn mouth size," in *Audio Engineering Society Convention*, Audio Engineering Society (1973).